LTE as a Potential Standard for Public Safety Indoor Body-to-Body Networks

Thijs Castel, Sam Lemey, Sam Agneessens,
Patrick Van Torre, Hendrik Rogier
INTEC Department
iMinds/Ghent University
Ghent, Belgium
thijs.castel@intec.ugent.be

Claude Oestges
ICTEAM, Catholic University of Louvain
Louvain-la-Neuve, Belgium
Claude.Oestges@UCLouvain.be

***Abstract*—In this paper, a wideband indoor body-to-body communication channel is characterized and analyzed into detail by means of the RMS delay spread and the 50% correlation bandwidth. These body-to-body channel parameters are calculated based on high-resolution power delay profiles, directly provided by the Elektrobit channel sounder, and are further analyzed using a ray tracing algorithm. We have replicated a real-life rescue operation, performed by two firefighters as part of the Rapid Intervention Team searching for potential victims, operating at the same floor of an office block. Both firefighters, who were simultaneously moving around in the vicinity of each other, were equipped with two cavity-backed Substrate Integrated Waveguide textile antennas unobtrusively integrated in the front and back section of their jackets, allowing us to analyze four independent body-to-body links. Furthermore, we prove that the Long Term Evolution (LTE) and, by extension, the LTE - Device to Device (LTE-D2D) standard is compatible with this indoor body-to-body channel. This could provide high data rate indoor communication between rescuers, enabling multimedia broadcast and realtime communication of on-body sensor data in public safety networks.**

***Index Terms*—Body-to-body communication, Long Term Evolution, Public Safety Networks**

I. Introduction

State-of the art narrowband public safety networks, such as TETRA [1], provide a wide variety of applications which help rescue workers to perform their jobs in an efficient manner and, hence, decrease the number of casualties. However, broadband networks could further improve life-critical communication by allowing high data rates, low latency and high spectral efficiency [2], [3], enabling multimedia broadcast and efficient communication of on-body sensor data. By providing realtime information to on-duty rescuers, their situational awareness increases, which strengthens their decision-making process and, hence, decreases the response time of operations. This can be of great importance when minutes, or even seconds, count.

Long Term Evolution (LTE) [4] is seen as the future mainstream cellular based network solution for public safety networks used by first responders. However, since highly reliable communication between the rescuers is required at any time, even when the cellular coverage fails or is not available, the LTE Device-to-Device (LTE-D2D) standard could be more suitable for indoor body-to-body communication between rescuers. This extension of the general LTE standard is defined as low-latency, energy-saving communication between two (on-body) User Equipment (UE) devices, in the proximity of each other, using an LTE air interface to set up a direct link without routing via an Evolved Node B (eNB) [5]. Therefore, in this contribution, we analyze if an indoor body-to-body network is compatible with LTE and, by extension, the LTE-D2D standard. Therefore, we performed wideband, indoor, body-to-body channel sounder measurements between two simultaneously moving firefighters, equipped with two integrated textile antennas, providing a sufficiently large set of reliable channel measurements to determine the wideband channel parameters, being the RMS delay spread and the 50% correlation bandwidth. These wideband channel parameters are then used to determine the pertinent Orthogonal Frequency Division Multiplexing (OFDM) parameters to verify the compatibility of the indoor environment with LTE, and, by extension, LTE-D2D.

When focussing on body-to-body communication, [6] and [7] present channel characterization for *narrowband* dynamic body-to-body communication channels at 2.45 GHz. Channel characterization of the *wideband* body-to-body transmissions by means of static and dynamic measurements, not replicating real life rescue scenarios, is described in [8]. Moreover, directional stacked patch antennas were mounted on the human body instead of the antennas being unobtrusively integrated into the clothing.

To the authors' best knowledge, this is the first paper which presents a detailed analysis of an indoor wideband body-to-body communication channel using high-resolution channel sounding measurements supplemented with ray-tracing results. Moreover, for the first time in literature, the paper validates, by means of real channel sounder measurements, that the LTE standard is very suitable for indoor body-to-body links between on-duty rescuers.

II. Measurement setup

Two Ultra Wideband cavity-backed slot antennas in Substrate Integrated Waveguide (SIW) technology [9] were unobtrusively integrated inside the front and back sections of rescuer workers' garments, as shown in Fig 1. The fabricated antenna is

matched for the frequency band ranging from 3.33 GHz to 4.66 GHz, with a -10 dB bandwidth of 1.33 GHz and a fractional bandwidth of 33%. Moreover, this topology provides stable radiation characteristics when placed on different on-body locations or even when the antenna is bent, which typically occurs in real-life rescue operations. Furthermore, owing to the use of a groundplane, the antenna radiates away from the firefighter while minimizing the backside radiation towards the firefighter's body which guarantees safe and energy-efficient operation and, hence, makes this antenna topology very suitable for on-body usage. Additionally, the fabricated SIW textile antenna is small, low-proflile, light weight and flexible. This enables easy deployment inside a rescuer's jacket.

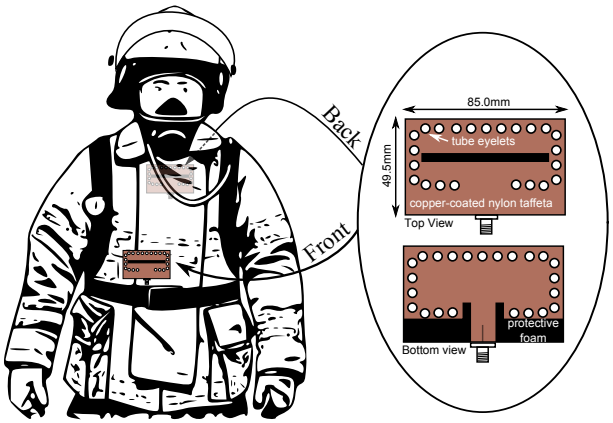

Fig. 1. Front and back locations of the two integrated UWB SIW textile antennas, for both the TX and RX firefighter.

A real-life rescue operation, performed by the Rapid Intervention Team looking for potential victims, was replicated by mobile measurements during which both firefighters were simultaneously moving around on the same floor of an office block. When both firefighters enter a building, according to the commonly employed "two in - two out" principle, the RX firefighter, whose trajectory is marked by the short dashed line on Fig. 2, starts scanning the offices whereas the TX firefighter, whose trajectory is marked by the long dashed line, is simultaneously scanning the hallway, while he remains in the vicinity of the RX firefighter. The markers A, B and C, placed along both firefighter trajectories, indicate where the firefighters are located at the same time instance during the one minute long measurement, gathering 4650 measurement cycles. Measurements were performed using the ULB-UCL Elektrobit channel sounder at 3.6 GHz center frequency with 120 MHz useful bandwidth. The TX power was chosen equal to 20dBm to obtain reliable wideband channel measurements.

III. Wideband channel characterization

Indoor body-to-body communication is heavily influenced by multiple delayed paths arriving at the RX firefighter, caused by several reflectors and scatterers in the office environment. The time varying power delay profiles $P_h(\tau)$, showing the power and the corresponding delays of these multipath components together with the power and the delay of the dominant, strongest path, are visualized in Fig. 3 for all four body-to-body links.

A number of interesting features are observed for the Front to Front (*F2F*) link when both firefighters are walking in the corridor (**interval BC** on Fig. 2) along the same positive X direction towards the end of the corridor. The last arriving multipath components, originating from the TX front antenna and impinging on the RX front antenna, decrease in delay, as seen on Fig. 3A. The opposite holds for the *B2B* link, as seen on Fig. 3D, in the same interval BC, where again, both firefighters are walking in the corridor (interval BC) along the same positive X direction towards the end of the corridor. Here, the dominant multipath component, transmitted by the TX back antenna and impinging on the RX back antenna, increases in delay and path length.

By modelling the indoor environment using the AWE Communication - Winprop ray tracing algorithm [10], we try to calculate the propagation paths of each multipath component in $P_h(\tau)$. Despite the fact that the office environment cannot be modelled into great detail because of the large number of potential reflectors and absorbers, such as computers, desks, people, which cannot all be included inside our model, good similarity is obtained between the power delay profile of the last measurement cycle in interval BC and by the ray tracing algorithm for the *F2F* as shown in Fig. 4. This good agreement is obtained by incorperating the most important scatterers on the simplied indoor office model, such as the metal and glass closets, windows, doors and walls, as also visible in Fig. 2.

The ray tracing algorithm shows that the last two dominant peaks for the *F2F* link are caused by multipath components that reflect on the metal closet and on the walls at the end of the corridor, as shown in Fig. 2, leading to decreasing delays when both firefighters are moving towards these reflectors, as in interval BC. For the *B2B* link, the ray tracing algorithm indicates that the last dominant multipath component corresponds to reflections on the window in the staircase leading to increasing delay and path loss when both firefighters are walking away from these reflectors, in the positive X-direction. For the *F2B* link, $P_h(\tau)$ changes dramatically over time due to multiple reflections, diffractions and scaterring. In contrast, for the *B2F* link, one multipath component remains constant over time as shown in Fig. 3C. The latter multipath component has a fairly constant delay because both firefighters are walking in the positive X-direction (as indicated in Fig. 2) at equal speeds, in a situation where the signal propagation occurs via double reflection on objects situated behind and in front of of the TX firefighter in the floor plan. Note that the power and delay of both the dominant path and multipath components vary over time, depending on the constantly changing mutual orientation and relative distance between the RX and the TX firefighters.

1) ***RMS delay spread****:* The RMS delay spread τ_{RMS} indicates the time domain spread of multiple delayed copies of the transmitted pulse arriving at the RX firefighter. It is calculated for every of the 4650 measurement cycles, for all four body-to-body links separately. Define L the number of distinct multipath components, P_l the (linear) power of a multipath

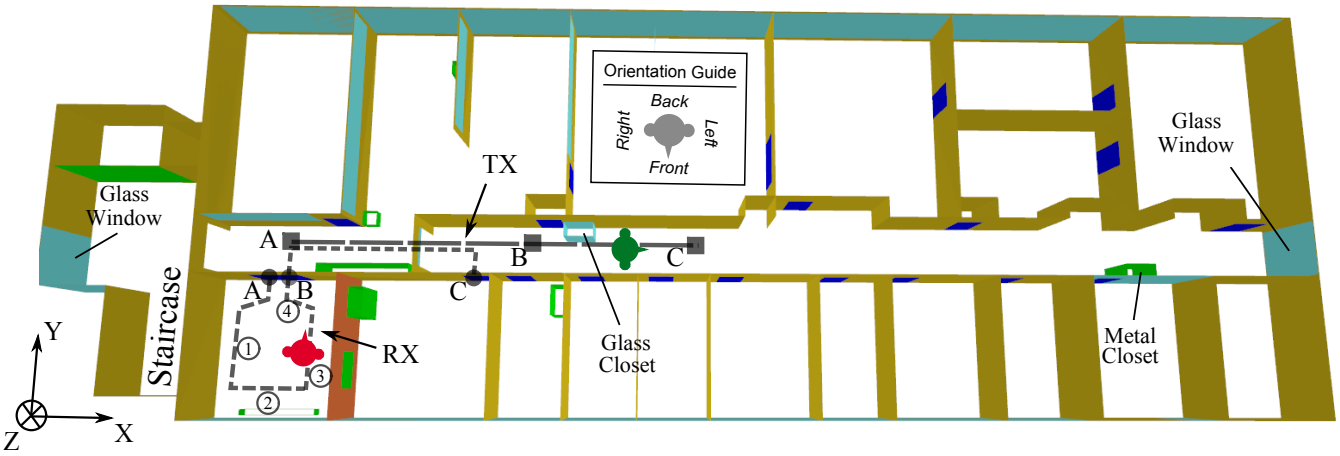

Fig. 2. Simplified indoor office model with the wideband body-to-body measurement scenario

component and τ_l the corresponding delay of that multipath component, such that the RMS delay spread τ_{RMS} is calculated via the mean delay $\bar{\tau}$ as [11]:

$$\bar{\tau} = \frac{\sum_{l=1}^{L} P_l.\tau_l}{\sum_{l=1}^{L} P_l}, \tag{1}$$

$$\tau_{RMS} = \sqrt{\frac{\sum_{l=1}^{L} P_l.(\tau_l - \bar{\tau})^2}{\sum_{l=1}^{L} P_l}} \tag{2}$$

The excess delay τ_{excess} is defined as the difference in delay between the first and last arriving multipath of $P_h(\tau)$. It is calculated as:

$$\tau_{excess} = \tau_L - \tau_1 \tag{3}$$

Since τ_{RMS} not only depends on the delay but also on the power of the multipath components, it is important to define the power ratio, in dB, as the ratio of the direct path power P_1 to the power summed over the other multipath components P_m, extracted from $P_h(\tau)$.

$$PR = 10.\log_{10}\left(\frac{P_1}{\sum_{m=2}^{L} P_m}\right) \tag{4}$$

By considering the power ratio, it is possible to distinguish indoor scenarios that lead to high and low τ_{RMS} values, such as in the **interval BC** for the F2B and the B2F link. As shown on Fig. 3B, for the F2B link, where the TX front and RX back antenna are pointing away from each other, a lot of multipath components are present in interval BC. The powers of these multipath components are only slightly smaller than the power of the dominant path, leading to a small power ratio and a large excess delay, which causes a high RMS delay spread, as shown in Fig. 5 and numerically described in Table I. In the same interval BC, the opposite holds for the B2F link, where the TX back antenna is directly pointing towards the RX front antenna. Now, the dominant, direct path is clearly stronger than the power in the multipaths, corresponding to a high mean power ratio but. Together with the smaller excess delay, this leads to a smaller τ_{RMS} in interval BC. When comparing the F2F and F2B link, we clearly notice the influence of the power ratio on τ_{RMS}. Despite the fact that the excess delay is approximately equal, the lower PR for the F2B link leads to a RMS delay spread that is 62% higher than for the F2F link, as described in Table I.

Fig. 5 also shows that, in **interval AB**, τ_{RMS} is low and approximately constant due to the lack of strong multipath components. Also note that τ_{RMS}, in Fig. 5, is obtained by using a running average filter over 77 consecutive samples, corresponding to one second of measurement, in order to prevent a heavily varying τ_{RMS} and to ensure that the trends are clearly visualized for all intervals.

TABLE I
MEAN POWER RATIO, MEAN EXCESS DELAY AND MEAN RMS DELAY SPREAD FOR **INTERVAL BC**

	$\overline{PR}(dB)$	$\overline{\tau}_{excess}(ns)$	$\overline{\tau}_{RMS}(ns)$
F2F	1.94	204	24.09
F2B	-5.51	201	39.18
B2F	14.61	115	6.85
B2B	2.32	159	18.11

Previous extensive wideband indoor channel measurements, described in [12], show that τ_{RMS} is environment and frequency dependent with values generally below 30 ns, except for very large rooms with large distances between potential reflectors, as is the case in our indoor environment. A more general rule of thumb indicates that τ_{RMS} is above 10 ns and under 50 ns [11] which largely matches the results presented in Fig. 6, presenting the CDFs of τ_{RMS} for all four body-to-body links, over the complete measurement duration.

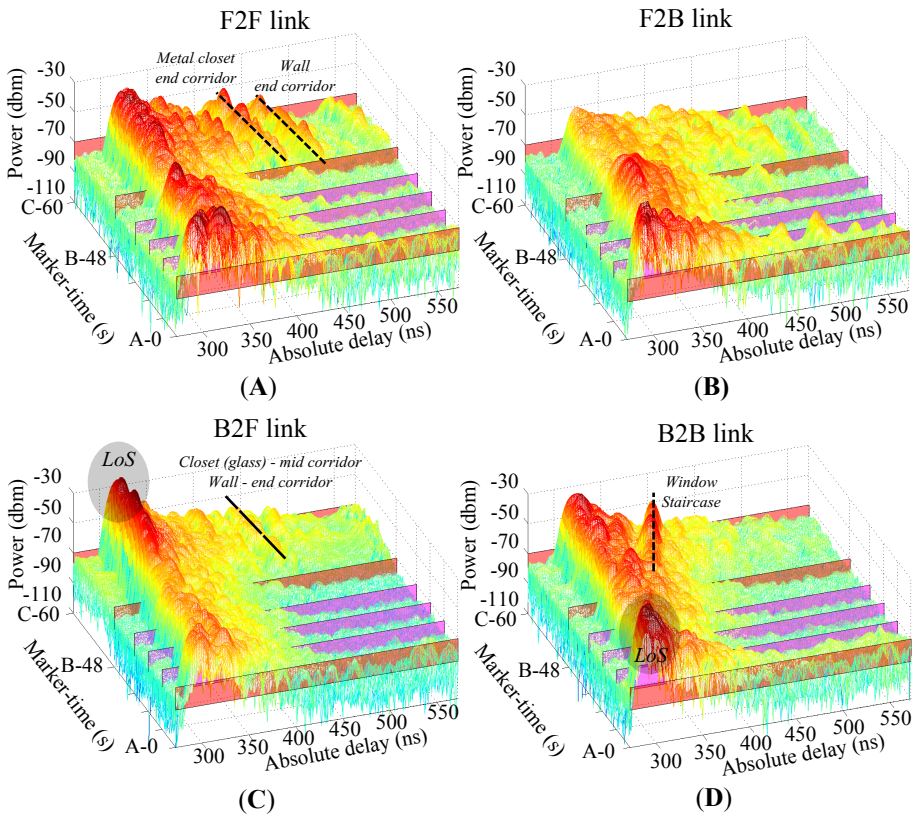

Fig. 3. Time varying power delay profiles $P_h(\tau)$ for all four body-to-body links

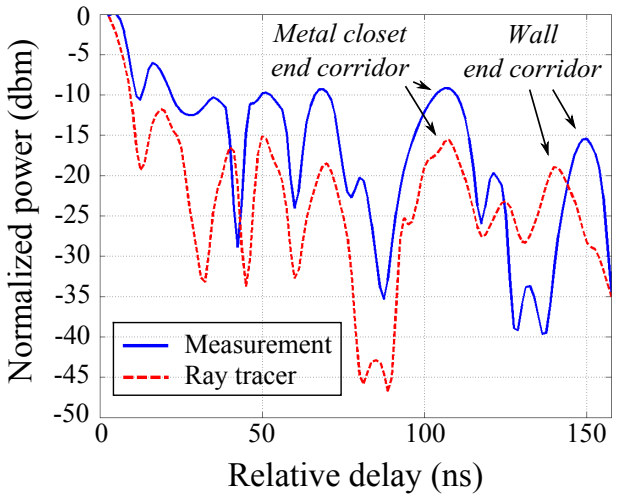

Fig. 4. Comparison of $P_h(\tau)$ obtained by the channel sounder measurement and calculated using the ray tracing algorithm for 1 cycle in interval BC for the F2F link

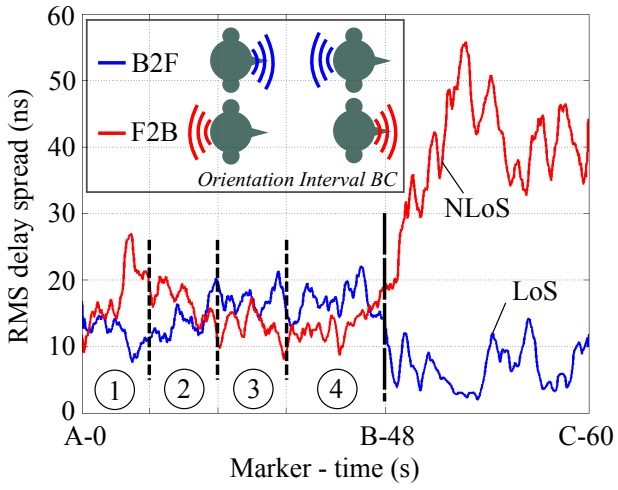

Fig. 5. RMS delay spread over time for the B2F and F2B link

For this indoor scenario, τ_{RMS} is above 1.71 ns and below 58.02 ns during 98% of all measurement cycles. Large variations in τ_{RMS} occur due to the constantly changing mutual orientations and the relative positions of both firefighters, as well as the varying distance between the two firefighters. The small τ_{RMS} values are caused by sporadic high values of the power ratio ($>$ 15dB), for example at the starting point (marker A) where the back antennas of both firefighter are close to each other, or by extremely low values of the excess delay ($<$ 50 ns). Low values for the excess delay sometimes occur when the received signal is very weak, leading to a dominant peak power only few dB above the noise floor. This leads to only a few multipath components exceeding the noise floor and hence to a small excess delay and a small τ_{RMS}. For further calculations in Section IV, we make use of the 90%

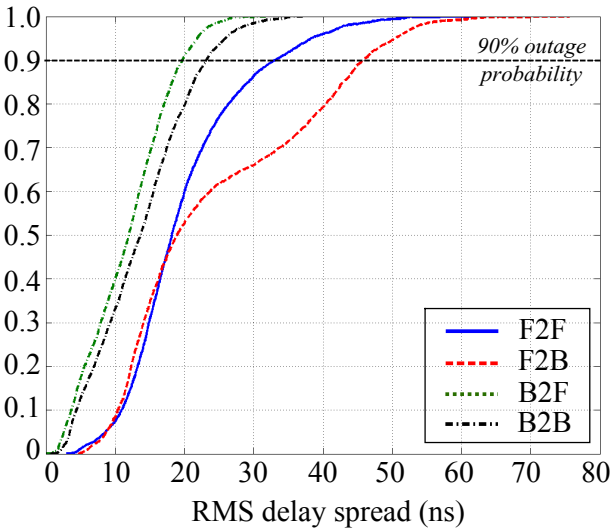

Fig. 6. CDF of τ_{RMS} over the compelete measurement for all four body-to-body links

outage probability level, $\tau_{RMS,90}$, defined as the maximum RMS delay spread during 90% of the time and these values are numerically described in Table II.

*2) **50% correlation bandwidth**:* If the calculated τ_{RMS} is not significantly smaller than the symbol duration T_S, strong multipath components of symbol X_n could influence symbol X_{n+1}, leading to Inter Symbol Interference (ISI). Moreover, delayed multipaths, arriving at the RX firefighter, introduce frequency selective fading, which is analyzed by observing the correlation between received signals at two different frequencies [11]. In this case, the frequency correlation function is given by the Fourier Transform of $P_h(\tau)$:

$$R_T(\Delta f) = \int_0^{\tau_{max}} P_h(\tau).e^{-j2\pi\Delta f\tau}.d\tau \qquad (5)$$

In this contribution, the 50% correlation bandwidth $B_{C,0.5}$ is defined as the minimal bandwidth separation Δf, resulting in 50% decorrelated signals. Note that, since the useful channel sounder bandwidth is equal to 120 MHz and the 50% correlation bandwidth is defined single-sided, the maximum computable bandwidth separation is limited to 60 MHz in our measurement setup.

If the indoor body-to-body channel only exhibits few weak multipath components, the wideband channel is almost frequency flat and the frequency separation is large ($>$ 60MHz). This is happening in the dashed red line in Fig. 7. In contrast, if the indoor body-to-body channel is composed of a lot of strong multipath components, corresponding to low power ratios, the frequency selectivity of the wideband channel increases because the delayed multipaths interfere with each other. This leads to smaller frequency separation to ensure 50% decorrelation, as happening for the solid blue line shown in Fig. 7, corresponding to to 13.81 MHz frequency separation for a Power Ratio equal to -6.89 dB.

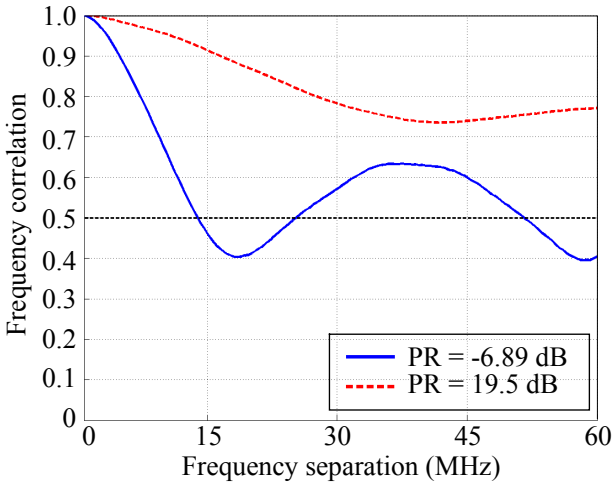

Fig. 7. Frequency correlation for two measurement cycles from the F2F link leading to a high and low Power Ratio (PR)

Fig. 8 shows the CDFs of $B_{C,0.5}$ for all four body-to-body links over the complete measurement. As stated before, the maximum computable $B_{C,0.5}$ is limited to 60 MHz because the useful Elektrobit channel sounder bandwidth is equal to 120 MHz. For further calculations in Section IV, we define the 10% outage probability level, $B_{C,0.5,10}$ as the minimum 50% correlation bandwidth during 90% of the time. These values are numerically described in Table II.

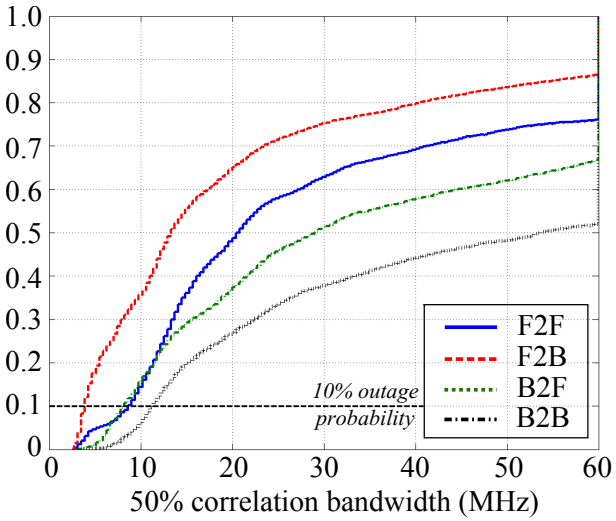

Fig. 8. CDF is $B_{C,0.5}$ over the complete measurement for all four body-to-body links

As a final step of the wideband body-to-body channel characterization, we calculate the parameter α which describes the inverse relationship between τ_{RMS} and $B_{C,0.5}$. Its value depends on the environment as well as on the power ratio:

$$\alpha = \frac{1}{\tau_{RMS}.B_{C,0.5}} \qquad (6)$$

Table II presents the mean α over all 4650 measurement cycles. Since α is generally between 1 and 10 for indoor

TABLE II
90% OUTAGE PROBABILITY OF THE RMS DELAY SPREAD ($\tau_{RMS,90}$), 10% OUTAGE PROBABILITY OF THE 50% CORRELATION BANDWIDTH ($B_{C,0.5,10}$) AND MEAN α

	F2F	F2B	B2F	B2B
$\tau_{RMS,90}(ns)$	33.07	45.80	19.69	23.18
$B_{C,0.5,10}(MHz)$	8.62	3.92	11.37	8.24
$\bar{\alpha}$	3.28	4.30	3.56	4.55

environments [12], these values indicate that the wideband, indoor body-to-body channel parameters are within the normal range.

IV. Long Term Evolution (LTE)

In this Section, we analyze whether the LTE standard, and, by extension, the LTE-D2D standard, would be suitable for an indoor body-to-body communication channel. As explained in Section III-2, the symbol duration T_s should be sufficiently larger than the RMS delay spread to avoid ISI. However, decreasing the symbol duration T_s results in a lower data rate, which limits the possibility to transmit multimedia or real-time on-body sensor data. Therefore, the frequency selective wideband channel is subdivided into *N* frequency-flat, orthogonal and low data rate subcarriers, which enlarges the total data rate and avoids ISI by inserting a cyclic prefix between two succesive OFDMA symbols on one subcarrier.

A. Frequency Domain

Define Δf_{max} as the maximum subcarrier bandwidth that still guarantees frequency flat fading on all subcarriers for all four body-to-body links during (at least) 90% of the time. Based on the minimum 50% correlation bandwidth, the maximum subcarrier spacing is generally calculated as [11]:

$$\Delta f_{max} = \frac{1}{10}.B_{C,0.5,min} = 392kHz \tag{7}$$

B. Time Domain

Define CP_{min} to be the minimum cyclic prefix length that prevents ISI on all subcarriers for all four body-to-body link during (at least) 90% of the time. Based on the maximum RMS delay spread, the minimal cyclic prefix length is generally calculated as [13]:

$$CP_{min} = 3.\tau_{RMS,max} = 137.4ns \tag{8}$$

These calculated OFDM parameters are compatible with the LTE standard, which sets the cyclic prefix length equal to 4.69 μs [14], being larger than the CP_{min}, and the subcarrier bandwidth equal to 15 kHz [14], being smaller than Δf_{max}.

V. Conclusion

This paper presents a detailed wideband indoor body-to-body channel characterization by means of channel sounder measurements and a ray tracing algorithm. The results of the measurement campaign shows that the LTE, and, by extension, the LTE-D2D standard is a potential standard for public safety indoor body-to-body networks.

Acknowledgment

The authors would like to thank IAP BESTCOM and UCL for providing the Elektrobit channel sounder and measurement locations.

References

[1] "ITU-R ," Digital Land Mobile Systems for Dispatch Traffic, Tech. Rep., 2012.

[2] "LTE-Advanced Evolution in Releases 12 - 14," Nokia Solutions and Networks white paper, Tech. Rep., 2015.

[3] "Public Safety Mobile Broadband," Ericsson white paper, Tech. Rep., 2014.

[4] T. Doumi, M. Dolan, S. Tatesh, A. Casati, G. Tsirtsis, K. Anchan, and D. Flore, "LTE for public safety networks," *Communications Magazine, IEEE*, vol. 51, no. 2, pp. 106–112, February 2013.

[5] X. Lin, J. G. Andrews, A. Ghosh, and R. Ratasuk, "An Overview on 3GPP Device-to-Device Proximity Services," *Communications Magazine, IEEE*, 2014.

[6] S. Cotton and W. Scanlon, "Channel characterization for single- and multiple-antenna wearable systems used for indoor body-to-body communications," *IEEE Transactions on Antennas and Propagation*, vol. 57, no. 4, pp. 980–990, April 2009.

[7] K. Ghanem, "Effect of Channel Correlation and Path Loss on Average Channel Capacity of Body-to-Body Systems," *IEEE Transactions on Antennas and Propagation*, vol. 61, no. 12, pp. 6260–6265, December 2013.

[8] Y. Wang, I. Bonev, J. Nielsen, I. Kovacs, and G. Pedersen, "Characterization of the indoor multiantenna body-to-body radio channel," *IEEE Transactions on Antennas and Propagation*, vol. 57, no. 4, pp. 972–979, April 2009.

[9] S. Lemey and H. Rogier, "SIW textile antennas as a novel technology for UWB RFID tags," in *Proceedings of RFID Technology and Applications Conference (RFID-TA)*. Tampere, Finland: IEEE, September 2014, pp. 256–260.

[10] AWE Communications - Wave Propagation and Radio Network Planning. [Online]. Available: http://www.awe-communications.com/

[11] R. Janaswamy, *Radiowave Propagation and Smart Antennas for Wireless Communications (The Springer International Series in Engineering and Computer Science)*. Springer, 2000.

[12] G. Janssen, P. Stigter, and R. Prasad, "Wideband indoor channel measurements and BER analysis of frequency selective multipath channels at 2.4, 4.75, and 11.5 GHz," *IEEE Transactions on Communications*, vol. 44, no. 10, pp. 1272–1288, October 1996.

[13] A. Goldsmith, *Wireless Communications*. Cambridge University Press, 2005.

[14] "3GPP LTE: Introducing Single-Carrier FDMA," Agilent Technologies, M. Rumney, Tech. Rep., 2008.